Response to Editor and Referees

Ms. Ref. No.: Egusphere-2025-2438

Title: Non-Stationary Dynamics of Compound Climate Extremes: A WRF-CMIP6-GAMLSS Framework for Risk Reassessment in Southeastern China

To Editor

Thank you very much for your time and consideration. We have carefully revised the manuscript according to the reviewers' comments and have now resubmitted the revised version together with a detailed response to all comments. We sincerely appreciate your guidance and the referees' constructive suggestions, which have significantly improved the quality of our manuscript. We would like to kindly inform you that there have been some changes in the affiliations of the manuscript authors. Specifically, Yinchi Zhang, who is currently funded by the China Scholarship Council (CSC), is now under the supervision of Professor Yi Wang at the University of Sussex in the UK. He has also made some contributions to the improvement of the manuscript. Additionally, due to a change in employment, Chao Deng has recently changed their institutional affiliation. We want to make you aware of these updates and kindly ask for your understanding.

To Anonymous Referee #1

Thank you for your thoughtful and detailed review of our manuscript. We greatly appreciate the time and effort you dedicated to providing feedback. Your constructive suggestions have been invaluable, and we will implement all changes in a revised version of the manuscript.

1.In the introduction, where you mention the need for fine-resolution models, you may need to add the reasons for the required high-resolution models for capturing compound extremes (e.g., local convective precipitation, spatial heterogeneity, …).

-Answer: Thank you for your comments. We have added a detailed description in lines 77-104 of the revised manuscript.

While large-scale studies play a crucial role in advancing our understanding of global climate change and extreme events, their practical relevance for disaster risk management and adaptation strategies in medium- and small-scale regions is relatively limited due to their lower spatial and temporal resolution. To overcome this constraint, dynamical downscaling, which utilizes nested

high-resolution regional climate models (RCMs), provides a critical technical pathway to investigate climate response mechanisms at fine-scales (Tapiador et al., 2020; Rahimi et al., 2024). Compared to Global Climate Models (GCMs), RCMs offer higher spatial resolution, allowing for more precise simulations of local climate effects induced by topography, such as local convective precipitation, orographic effects, and regional climate heterogeneity (Gilbert et al., 2025). In regions with complex terrain, RCMs are particularly effective at capturing spatial variations of climate variables, such as the differences in wind patterns, precipitation, and their distribution caused by topography in mountainous or basin areas (Imran and Evans, 2025). For example, Byun et al. (2023) assessed the ability of RCMs and GCMs to simulate storm tracks in East Asia, revealing that RCMs are better able to capture high-resolution topography, thereby reducing the biases found in GCMs. Lin et al. (2022) showed that RCMs driven by ERA-Interim reanalysis data are capable of capturing small-scale processes, such as orographic effects, and outperform GCMs in reproducing the large-scale features of the Heat Wave Magnitude Index-daily. Torrez-Rodriguez et al. (2023) also demonstrated that RCMs are better at reproducing the main spatio-temporal characteristics of precipitation in subtropical complex terrain regions. As an advanced convection-permitting RCM, the WRF model significantly enhances the simulation capability for meteorological processes at 1-10 km scales through its fully compressible, non-hydrostatic dynamic core framework (Talbot et al., 2012). This high-resolution simulation capability gives the WRF model a unique advantage in capturing small-scale meteorological phenomena. Zhou et al. (2024) developed a 9 km resolution regional reanalysis dataset covering the Tibetan Plateau based on the WRF model, and demonstrated its superior applicability compared to the fifth generation European Centre for Medium-Range Weather Forecasts Reanalysis (ERA5). Yang et al. (2024) revealed that the WRF model provides better accuracy in simulating snow depth during the cold season in high-elevation regions compared to ERA5-Land.

2.May you please check the following articles and discuss how you improve their work and what your innovation is compared to it? https://link.springer.com/article/10.1007/s00382-020-05538-2

-Answer: Thank you for your insightful comment regarding the comparison of our work with the study by Singh et al. (2021) on non-stationary compound extreme events (CCEs). Compared to the study by Singh et al. (2021), our research offers significant innovations in both spatial scale and

methodology. Firstly, while Singh et al. (2021) focus on large-scale ensemble simulations to analyze compound extreme events in Canada, our study targets the medium-to-small scale of the Minjiang River Basin (MRB), a region characterized by complex monsoonal climates and varied topography. By employing high-resolution dynamic downscaling with the WRF model, we are able to conduct a finer-scale risk assessment of compound extreme events and their spatial heterogeneity, thus providing a more localized approach to evaluate the impacts of climate change. Secondly, in terms of methodology, Singh et al. (2021) use a Bayesian Copula model to analyze the dependence structure between temperature and precipitation. In contrast, we introduce the Generalized Additive Model for Location Scale and Shape (GAMLSS) to capture non-stationary changes and assess the risk of compound extremes. The GAMLSS model allows us to simultaneously account for variations in both the mean and variance of climate variables, offering a more comprehensive and detailed framework for risk assessment. Furthermore, we have referenced this study in lines 511-513 of the discussion section.

Singh et al. (2021) demonstrated that under climate change, precipitation and temperature exhibit a non-stationary dependent structure, and treating them independently can substantially underestimate the occurrence of compound extremes.

3.May you make a list of the 18 climate models you applied for your study in the supplementary file?

-Answer: Thank you for your suggestion. We have provided a list of the 18 models used in the bias-corrected CMIP6 dataset (Xu et al., 2021) in the supplementary file as requested.

Table S1 CMIP6 models used in CMIP6bc.

No.	Model	Institution	Approximate grid spacing
1	ACCESS-CM2	Commonwealth Scientific and Industrial Research Organisation (Australia)	1.875° × 1.25°
2	ACCESS-ESM1–5	Commonwealth Scientific and Industrial Research Organisation (Australia)	1.875° × 1.25°
3	CanESM5	Canadian Centre for Climate Modelling and Analysis (Canada)	2.81° × 2.81°
4	BCC-CSM2-MR	Beijing Climate Center (China)	1.125° × 1.125°
5	FGOALS-f3-L	Institute of Atmospheric Physics, Chinese Academy of Sciences (China)	1.25° × 1°
6	FGOALS-g3	Institute of Atmospheric Physics, Chinese Academy of Sciences (China)	2° × 2.25°
7	EC-Earth3	European EC-Earth Consortium (Europe)	0.70° × 0.70°
8	EC-Earth3-Veg	European EC-Earth Consortium (Europe)	0.70° × 0.70°
9	IPSL-CM6A-LR	Institute Pierre Simon Laplace (France)	2.5° × 1.26°
10	AWI-CM-1-1-MR	Alfred Wegener Institute, Helmholtz Centre for Polar and Marine Research (Germany)	0.94° × 0.94°
11	MPI-ESM1-2-HR	Max Planck Institute for Meteorology (Germany)	0.94° × 0.94°
12	MPI-ESM1-2-LR	Max Planck Institute for Meteorology (Germany)	1.875° × 1.875°
13	MIROC6	Japan Agency for Marine-Earth Science and Technology (Japan)	1.41° × 1.41°
14	MRI-ESM2-0	Meteorological Research Institute, Japan Meteorological Agency (Japan)	1.125° × 1.125°
15	NorESM2-LM	Norwegian Climate Center (Norway)	2.5° × 1.875°
16	CESM2	Climate and Global Dynamics Laboratory, National Center for Atmospheric Research (USA)	1.25° × 0.94°
17	CESM2-WACCM	Climate and Global Dynamics Laboratory, National Center for Atmospheric Research (USA)	1.25° × 0.94°
18	GFDL-ESM4	Geophysical Fluid Dynamics Laboratory, National Oceanic and Atmosphere Administration (USA)	1.25° × 1.0°

4.You mentioned that “The dataset used in this study covers the historical period (2005–2014)”, why did you choose only 10 years as historical data?

-Answer: Thank you for your comment. We have provided an explanation for this issue in lines 212-217 of the revised manuscript.

Despite its widespread application in previous studies (Jamal et al., 2023; Huang et al., 2024; Wu and Zheng, 2023), we conduct a 10-year validation over the MRB. Considering both the reliability of the dataset and the need to optimize computational resources (simulating one year over the MRB requires approximately four days on 80 CPU cores), we select a 10-year historical period (2005–2014) as sufficient to demonstrate the reliability of the CMIP6bc dataset for driving the WRF simulations.

5.Why did you only use SSP2-4.5 and SSP5-8.5? Why not SSP1-2.6?

-Answer: Thank you for your insightful comment. The reason we focused on SSP2-4.5 and SSP5-8.5 scenarios is that the bias-corrected dataset we used (Xu et al., 2021) only provides data for these two scenarios. This limitation is due to the specific selection of SSP scenarios made during the dataset development. We speculate that the dataset creators aimed to highlight the differences between the moderate and high-emission scenarios, particularly to emphasize the potential impacts of future climate changes under these contrasting pathways. By focusing on SSP2-4.5 (moderate emission scenario) and SSP5-8.5 (high-emission scenario), the dataset offers a clear comparison of how differing levels of greenhouse gas emissions can influence climate projections, especially in terms of temperature rise, extreme events, and other key climate variables. Although SSP1-2.6, which represents a low-emission scenario, is also highly relevant, it may not have been included to maintain the dataset's focus on the more critical scenarios that are likely to dominate future climate projections.

6.Please make clearer how the downscaling integrates with your GAMLSS framework.

-Answer: Thank you for your comment. We have provided additional information on this issue in lines 125-131 of the revised manuscript.

To address these research gaps, this study adopts a high-resolution approach by integrating the WRF model with GAMLSS. We first perform dynamical downscaling using the WRF model to refine the bias-corrected Coupled Model Intercomparison Project Phase 6 (CMIP6bc) data (1.25° ×

1.25°) to a 3 km resolution. Based on these high-resolution WRF outputs, CCEs are then identified and used as input for the GAMLSS framework to analyze their non-stationary characteristics. This methodology overcomes the limitations of traditional coarse-resolution models and addresses the shortcomings of stationary assumptions in CCE analysis.

7.Please make it clear what you mean by "enhanced" or "advanced" GAMLSS in the manuscript. Do you mean the GAMLSS, which considers non-stationary characteristics?

-Answer: Thank you for your question. We have provided a detailed explanation of this issue in lines 274-289 of the revised manuscript.

In the GAMLSS model, time (year) is used as the independent variable (x), and the number of days per year for each type of CCE is treated as the dependent variable (y), thereby enabling the calculation of the non-stationary characteristics of each CCE. We employ two types of GAMLSS models to capture potential changes in the distribution of meteorological variables. The first is the traditional two-parameter location–scale model (mean μ and variance σ), which assumes a fixed distributional shape. The second is a more flexible four-parameter location–scale–shape model (mean μ, variance σ, skewness ν, and kurtosis τ), allowing the distributional shape to evolve over time. These extended models retain the mean and variance parameters while incorporating two additional shape parameters to capture asymmetry and tail behavior. We assess the models by comparing their goodness of fit and select the one that best represents the data distribution for subsequent analyses. Regarding the calculation of stationarity, we consider the CCEs to be stationary if both the mean and variance remain stable. If either the mean or variance shows significant variation, the CCEs are considered non-stationary. Supplement Table S12 lists all the distribution functions implemented in our study. The R code for implementing GAMLSS model can be accessed at https://github.com/gamlss-dev/gamlss.

8.In the supplementary file, please provide a table showing the validation results.

-Answer: Thank you for your comment. We have added this section of content to the supplementary file. Table S3 Meteorological stations information.

ID	Name	Longitude (°N)	Latitude (°E)	Elevation (m)
1	Jiuxianshan	118.1	25.72	1653.5
2	Gutian	118.73	26.58	361.5
3	Datian	117.83	25.7	400.1
4	Youxi	118.15	26.17	126.1
5	Dehua	118.23	25.48	521.4
6	Yongtai	118.93	25.87	85.6
7	Fuzhou	119.28	26.08	83.8
8	Changle	119.5	25.97	4.1
9	Minhou	119.15	26.15	57.8
10	Minqing	118.85	26.23	40.8
11	Sanming	117.62	26.27	215
12	Ninghua	116.63	26.23	358.9
13	Yongan	117.35	25.97	206
14	Shaxian	117.8	26.4	120.6
15	Qingliu	116.85	26.2	310.6
16	Liancheng	116.75	25.72	380.0
17	Guangze	117.3	27.52	265.4
18	Nanping	118.17	26.65	125.6
19	Jiangle	117.47	26.73	154.7
20	Jianning	116.85	26.83	342.3
21	Shaxi	117.15	26.4	357.4
22	Taining	117.17	26.9	342.9
23	Shaowu	117.47	27.33	191.5
24	Shunchang	117.8	26.8	175.2
25	Jianou	118.31	27.05	154.9
26	Jianyang	118.12	27.33	196.9
27	Zhenghe	118.82	27.37	221.5
28	Songxi	118.8	27.52	205.4
29	Wuyishan	118.03	27.77	220.6
30	Pucheng	118.53	27.92	276.9

Table S4 Temperature simulation results based on ERA5

Station	STD	RMSE	CC
Jiuxianshan	1.14	0.59	0.99
Gutian	0.98	0.29	0.99
Datian	0.97	0.07	1.00
Youxi	0.99	0.23	0.99
Dehua	0.98	0.20	0.99
Yongtai	1.00	0.22	0.99
Fuzhou	0.97	0.26	0.98
Changle	0.92	0.20	0.98
Minhou	0.97	0.35	0.95
Minqing	0.98	0.16	0.99
Sanming	1.03	0.30	0.99
Ninghua	0.99	0.12	0.99
Yongan	1.01	0.32	0.99
Shaxian	1.03	0.36	0.99
Qingliu	0.96	0.14	0.99
Liancheng	1.01	0.27	0.99
Guangze	1.01	0.19	0.99
Nanping	1.02	0.29	0.99
Jiangle	1.02	0.29	0.99
Jianning	1.02	0.19	0.99
Shaxi	0.97	0.26	0.99
Taining	0.99	0.21	0.99
Shaowu	1.03	0.31	0.99
Shunchang	1.03	0.32	0.99
Jianou	0.78	0.25	0.99
Jianyang	0.75	0.36	0.99
Zhenghe	1.01	0.14	0.99
Songxi	0.99	0.14	0.99
Wuyishan	0.82	0.27	1.00
Pucheng	1.05	0.26	0.99

Table S5 Temperature simulation results based on CMIP6bc

Station	STD	RMSE	CC
Jiuxianshan	1.10	0.66	0.96
Gutian	0.96	0.37	0.97
Datian	0.94	0.29	0.96
Youxi	0.95	0.30	0.96
Dehua	0.97	0.30	0.96
Yongtai	0.96	0.29	0.96
Fuzhou	0.96	0.32	0.96
Changle	0.88	0.28	0.96
Minhou	0.53	0.68	0.96
Minqing	0.94	0.27	0.96
Sanming	0.97	0.37	0.96
Ninghua	0.93	0.25	0.97
Yongan	0.95	0.30	0.96
Shaxian	0.96	0.33	0.97
Qingliu	0.91	0.26	0.97
Liancheng	0.93	0.32	0.96
Guangze	0.96	0.28	0.98
Nanping	0.98	0.37	0.97
Jiangle	0.95	0.27	0.97
Jianning	0.96	0.28	0.98
Shaxi	0.92	0.33	0.97
Taining	0.94	0.28	0.97
Shaowu	0.95	0.27	0.97
Shunchang	0.95	0.30	0.97
Jianou	0.79	0.32	0.97
Jianyang	0.73	0.41	0.97
Zhenghe	0.95	0.25	0.97
Songxi	0.94	0.25	0.97
Wuyishan	0.81	0.35	0.97
Pucheng	0.95	0.24	0.98

Table S6 Precipitation simulation results based on ERA5

Station	STD	RMSE	CC
Jiuxianshan	1.20	0.71	0.80
Gutian	1.13	0.55	0.87
Datian	1.20	0.71	0.81
Youxi	1.35	0.72	0.86
Dehua	1.16	0.64	0.83
Yongtai	1.04	0.69	0.78
Fuzhou	0.94	0.75	0.74
Changle	0.76	0.89	0.62
Minhou	1.04	0.79	0.73
Minqing	1.10	0.65	0.81
Sanming	0.98	0.61	0.81
Ninghua	1.18	0.74	0.78
Yongan	1.12	0.61	0.84
Shaxian	0.97	0.56	0.84
Qingliu	1.16	0.72	0.79
Liancheng	1.36	0.89	0.75
Guangze	1.24	0.51	0.92
Nanping	0.97	0.53	0.85
Jiangle	1.07	0.45	0.91
Jianning	1.12	0.69	0.79
Shaxi	1.01	0.57	0.84
Taining	1.11	0.46	0.91
Shaowu	1.35	0.82	0.80
Shunchang	1.06	0.51	0.88
Jianou	0.96	0.54	0.85
Jianyang	0.99	0.46	0.89
Zhenghe	1.06	0.44	0.91
Songxi	1.17	0.55	0.89
Wuyishan	1.23	0.48	0.93
Pucheng	1.06	0.59	0.84

Table S7 Precipitation simulation results based on CMIP6bc

Station	STD	RMSE	CC
Jiuxianshan	1.19	0.98	0.61
Gutian	1.12	0.92	0.63
Datian	1.38	1.05	0.65
Youxi	1.11	0.85	0.68
Dehua	1.06	0.83	0.69
Yongtai	0.94	0.97	0.52
Fuzhou	0.94	0.94	0.57
Changle	0.82	0.70	0.73
Minhou	0.93	0.96	0.54
Minqing	1.16	0.97	0.60
Sanming	1.10	0.84	0.68
Ninghua	1.12	0.81	0.71
Yongan	1.26	1.04	0.59
Shaxian	0.97	0.82	0.66
Qingliu	1.23	0.98	0.63
Liancheng	1.31	1.11	0.56
Guangze	1.13	0.86	0.68
Nanping	0.98	0.75	0.71
Jiangle	1.13	0.84	0.69
Jianning	1.06	0.88	0.64
Shaxi	1.26	0.96	0.67
Taining	1.16	0.89	0.66
Shaowu	1.15	0.92	0.64
Shunchang	1.11	0.78	0.73
Jianou	1.01	0.80	0.68
Jianyang	1.13	0.89	0.65
Zhenghe	1.11	0.96	0.59
Songxi	1.15	0.90	0.66
Wuyishan	1.18	0.83	0.72
Pucheng	1.11	0.80	0.71

9.In the results and discussion, I could not find how the results show that considering the non-stationary characteristics leads to better or more reliable results. May you compare the results with previous studies in which the time series was assumed to be stationary?

-Answer: Thank you for the constructive comment. We have enriched our discussion section by comparing our results with previous studies in the revised manuscript, specifically in lines 501-519. Within the GAMLSS framework, we constructed both stationary and non-stationary models and evaluated their performance using the Akaike Information Criterion (AIC), adhering to the established principle that a smaller AIC value indicates a better model fit. The results show that, compared to the stationary model, the non-stationary model occupies more grid points (i.e., has a lower AIC value), indicating its stronger ability to adapt to the characteristics of the time series (Figure 6). Furthermore, the comparative analysis of the return period results between the two models (Figure 8) shows that the non-stationary model exhibits more extreme trends in compound extreme events (CEEs), reinforcing the importance of accounting for non-stationarity in such analyses. Additionally, the subsequent evaluation using the Filliben coefficient confirmed the goodness-of-fit of the selected models (Figure S3), further validating our approach. We would like to clarify that the statement in the original manuscript claiming that the "non-stationary model is better than the stationary model" is misleading. A more accurate description is that the non-stationary model is more appropriate when accounting for temporal trends and mean-state changes, whereas the stationary model tends to underestimate the recurrence risk of CCEs based on the results.

4.3 Frequency of recurrence systematically underestimated by stationary model

Our comparison between stationary and non-stationary model indicates that the latter captures a significant increase in recurrence risks, particularly for 100-year CCEs, which are projected to rise by 3.12 days per decade under the SSP5-8.5 scenario. Stationary model systematically underestimates recurrence frequency after 2045, and the stronger non-stationary response of 100-year events highlights the heightened vulnerability of high-impact, low-probability extremes. Additionally, the west-to-east gradient in recurrence frequency, with hotspots in the Shaxi River Basin, may be attributed to topographic and land-surface heterogeneity, which modulate local hydroclimatic responses (Zheng et al., 2023). Previous studies have similarly shown that

conventional extreme value models fail to capture the escalating severity of extreme events under climate change. Singh et al. (2021) demonstrated that under climate change, precipitation and temperature exhibit a non-stationary dependent structure, and treating them independently can substantially underestimate the occurrence of compound extremes. Feng et al. (2020) compared the recurrence probabilities of floods under stationary and non-stationary conditions and found that, under non-stationary conditions, the annual variability of floods is significantly greater. Xu et al. (2025) evaluated changes in global marine heatwaves and found that stationary models significantly underestimate their frequency, intensity, and duration. In summary, these studies collectively highlight that accounting for non-stationarity is crucial for accurately assessing various extreme events.

10.The English language also should be assessed more carefully.

-Answer: Thank you for your comment. We have carefully revised and polished the English language in the manuscript to improve clarity and readability.

To Anonymous Referee #2

We sincerely appreciate your thorough and constructive comments, which have been instrumental in improving our manuscript. We also apologize for the lack of clarity in the introduction and methodology sections of the manuscript, and we assure you that these issues have be addressed in the revised version. Please find the detailed point-by-point responses below.

Major Comments:

1.Throughout the manuscript (and also in the title), the authors state that this study addresses the 'risk' of CCEs. As risk assessment typically involves an (monetary) impact analysis (see e.g. UNDRR (2007) for the definition of natural hazard risk), it may be more accurate to frame the study in terms of frequency changes or recurrence, which the authors mentioned somewhere in the manuscript. Therefore, I recommend carefully reviewing and revising all uses of "risk" or "risk assessment" to avoid overstating the study's scope.

-Answer: We fully agree with and appreciate your suggestion regarding the use of the term "risk." As the reviewer pointed out, risk assessment typically involves an analysis of impacts, particularly economic or social impacts. From the perspective of disaster-inducing factors (hazard), we have not delved into analyzing the exposure of disaster-bearing bodies (such as society, ecosystems, etc.) and their capacity to withstand these impacts. Therefore, we have revised the title and related statements in the revised manuscript to more accurately reflect the actual content and scope of our study. Specifically, we have removed the phrase "Risk Reassessment" from the title, and the revised title is: 'Non-Stationary Dynamics of Compound Climate Extremes: A WRF-CMIP6-GAMLSS Framework for Southeastern China.' Additionally, we have replaced the term "risk" with "frequency" throughout the manuscript.

2.While research gaps are introduced in L60-62, they require clearer identification. There are a number of studies looking into the frequency changes in compound events, both in China and other parts of the world. To name a few: Zscheischler et al. (2018), Fang et al. (2025) npj climate and atmospheric science, Wu et al. (2023) Earth's Future, Ridder et al. (2022) npj climate and atmospheric science, and so on. How does the present study compare or advance beyond these works?

-Answer: Thank you for your feedback. We have compared our study with previous research in

lines 66-76 of the revised manuscript and have clarified our innovations in lines 77-80 and 121-131.

Recent studies have increasingly focused on CCEs, highlighting their growing significance in the context of climate change. Zscheischler et al. (2018) were the first to clearly define the concept of compound events, emphasizing how the interaction of multiple climate and meteorological drivers can amplify extreme impacts. Building on this, Ridder et al. (2022) conducted the first global-scale assessment of the changes in compound events, specifically examining the co-occurrence of heatwaves and drought, extreme winds, and precipitation. Wu et al. (2023) revealed that under warming conditions, the risks associated with global compound pluvial–hot extreme events are projected to be significantly greater in the future than those observed during the historical period. Fang et al. (2025) investigated the future changes of sequential heatwaves and precipitation events as well as concurrent drought and heatwave events in China, with projections indicating an increase in both the frequency and intensity of these events.

While large-scale studies play a crucial role in advancing our understanding of global climate change and extreme events, their practical relevance for disaster risk management and adaptation strategies in medium- and small-scale regions is relatively limited due to their lower spatial and temporal resolution. *To overcome this constraint, dynamical downscaling, which utilizes nested high-resolution regional climate models (RCMs), provides a critical technical pathway to investigate climate response mechanisms at fine-scales (Tapiador et al., 2020; Rahimi et al., 2024). Compared to Global Climate Models (GCMs), RCMs offer higher spatial resolution, allowing for more precise simulations of local climate effects induced by topography, such as local convective precipitation, orographic effects, and regional climate heterogeneity (Gilbert et al., 2025). In regions with complex terrain, RCMs are particularly effective at capturing spatial variations of climate variables, such as the differences in wind patterns, precipitation, and their distribution caused by topography in mountainous or basin areas (Imran and Evans, 2025). For example, Byun et al. (2023) assessed the ability of RCMs and GCMs to simulate storm tracks in East Asia, revealing that RCMs are better able to capture high-resolution topography, thereby reducing the biases found in GCMs. Lin et al. (2022) showed that RCMs driven by ERA-Interim reanalysis data are capable of capturing small-scale processes, such as orographic effects, and*

outperform GCMs in reproducing the large-scale features of the Heat Wave Magnitude Index-daily. Torrez-Rodriguez et al. (2023) also demonstrated that RCMs are better at reproducing the main spatio-temporal characteristics of precipitation in subtropical complex terrain regions. As an advanced convection-permitting RCM, the WRF model significantly enhances the simulation capability for meteorological processes at 1-10 km scales through its fully compressible, non-hydrostatic dynamic core framework (Talbot et al., 2012). This high-resolution simulation capability gives the WRF model a unique advantage in capturing small-scale meteorological phenomena. Zhou et al. (2024) developed a 9 km resolution regional reanalysis dataset covering the Tibetan Plateau based on the WRF model, and demonstrated its superior applicability compared to the fifth generation European Centre for Medium-Range Weather Forecasts Reanalysis (ERA5). Yang et al. (2024) revealed that the WRF model provides better accuracy in simulating snow depth during the cold season in high-elevation regions compared to ERA5-Land. Additionally, traditional extreme event analyses rely on stationarity assumptions (when analyzing time series data, it is assumed that the statistical properties of the series remain constant over time), presuming that the probability and distributional parameters of climate variables are constant (Sun et al., 2018; Nerantzaki et al., 2023). However, driven by synergistic effects of global warming and anthropogenic forcing, extremes exhibit significant shifts in distributional characteristics (Gao et al., 2018). Therefore, traditional models fail to capture the non-stationary (the statistical properties of a time series change over time and do not remain constant) changes in these extreme events. Many studies have applied the Generalized Additive Models for Location, Scale, and Shape (GAMLSS) (Rigby and Stasinopoulos 2005) to address non-stationary problems in hydrological and meteorological extremes, enabling updated risk analysis of evolving climate extremes. Lei et al. (2021) investigated the non-stationary changes of extreme precipitation in the Poyang Lake Basin and found that the stationary assumption underestimates the intensity of extreme precipitation in this region. Shao et al. (2022) innovatively proposed the Nonstationary Standardized Runoff Index (NSRI), and the results indicate that, compared to the stationary index, it can more accurately identify drought events. Salarijazi et al. (2023) evaluated the nonstationarity of maximum temperatures in multiple urban areas of Iran and concluded that traditional stationary approaches tend to underestimate the risk of annual maximum temperatures. ***However, existing non-stationary***

analyses only focus on individual extremes, and the potential non-stationarity of CCEs has not been established. The comprehensive assessment of future changes in CCEs within a non-stationary framework is also lacking.

To address these research gaps, this study adopts a high-resolution approach by integrating the WRF model with GAMLSS. We first perform dynamical downscaling using the WRF model to refine the bias-corrected Coupled Model Intercomparison Project Phase 6 (CMIP6bc) data (1.25° × 1.25°) to a 3 km resolution. Based on these high-resolution WRF outputs, CCEs are then identified and used as input for the GAMLSS framework to analyze their non-stationary characteristics. This methodology overcomes the limitations of traditional coarse-resolution models and addresses the shortcomings of stationary assumptions in CCE analysis.

3.Fig. 1 outlines the key methodological steps in this study. Many unintroduced acronyms e.g. WRFOUT, CC and PBIAS are used without prior explanation, which may reduce the readability and understanding of the framework.

-Answer: We appreciate your suggestion and have revised Figure 1 in the updated manuscript to enhance its readability for the readers.

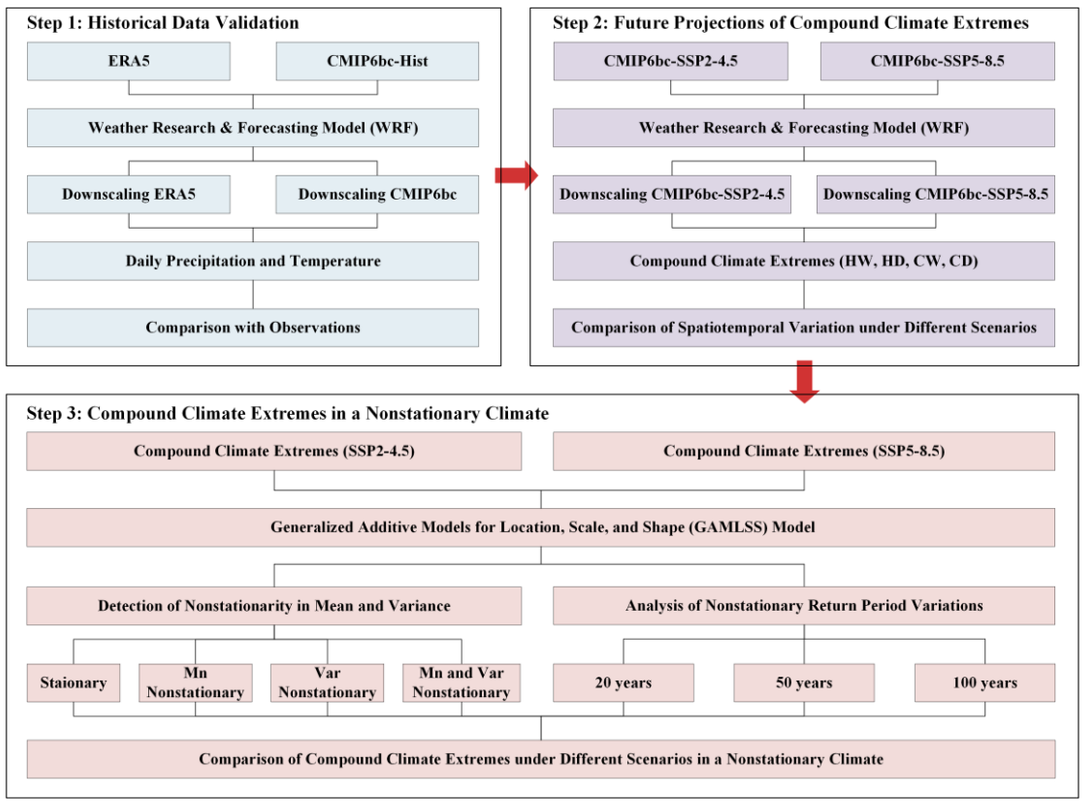

Figure 1. Flowchart of CCEs projection in a non-stationary framework.

4.Please elaborate on the types of CCEs commonly occurring during the flood season (Line 99). Including examples of historical events would help illustrate this.

Thank you for your suggestion. We have addressed this issue in lines 192-200 of the revised manuscript.

The basin displays spatio-temporal heterogeneity in precipitation, with flood seasons from April to September that often accompany CCEs. Particularly in the late flood season (July to September), the MRB experiences frequent typhoon-related compound disasters: the upper and middle reaches are commonly affected by typhoon-rainstorm-landslide events, while the lower reaches face high occurrences of typhoon-rainstorm-urban waterlogging and typhoon-rainstorm-flood events (Yang et al., 2025). In 2023, for example, typhoon Doksuri (No. 2305) caused approximately 66,794 people to be affected in Fuzhou, the downstream city of the MRB, with direct economic losses reaching 588 million RMB (Yan et al., 2024). In addition, the region also exhibits a climate characteristic of concurrent rainfall and heat, with CCEs frequently occurring during the warm season, driven by high temperature and heavy rainfall (Sun et al., 2025).

5.Section 2 provides a description of critical methodological steps of this work; however, they lack sufficient detail to fully convey its approach and practical implementation. I suggest to clarify the following concerns:

a.For validation of historical simulation results:

i.Why is the validation only focused on a 10-year period (2005–2014)?

-Answer: Thank you for your comment. We have provided an explanation for this issue in lines 212-217 of the revised manuscript.

Despite its widespread application in previous studies (Jamal et al., 2023; Huang et al., 2024; Wu and Zheng, 2023), we conduct a 10-year validation over the MRB. Considering both the reliability of the dataset and the need to optimize computational resources (simulating one year over the MRB requires approximately four days on 80 CPU cores), we select a 10-year historical period (2005–2014) as sufficient to demonstrate the reliability of the CMIP6bc dataset for driving the WRF simulations.

ii.Why would the ERA5 serve as the benchmark not the observed data (L113-115)?

-Answer: Thank you for your question. We would like to clarify that, in fact, we have three sets of data: observed data, WRF-ERA5, and WRF-CMIP6bc. ERA5, as a widely used WRF-driven

dataset, is utilized here as a reference for the simulation results. Indeed, the actual validation data comes from the meteorological station observations (Figure S1).

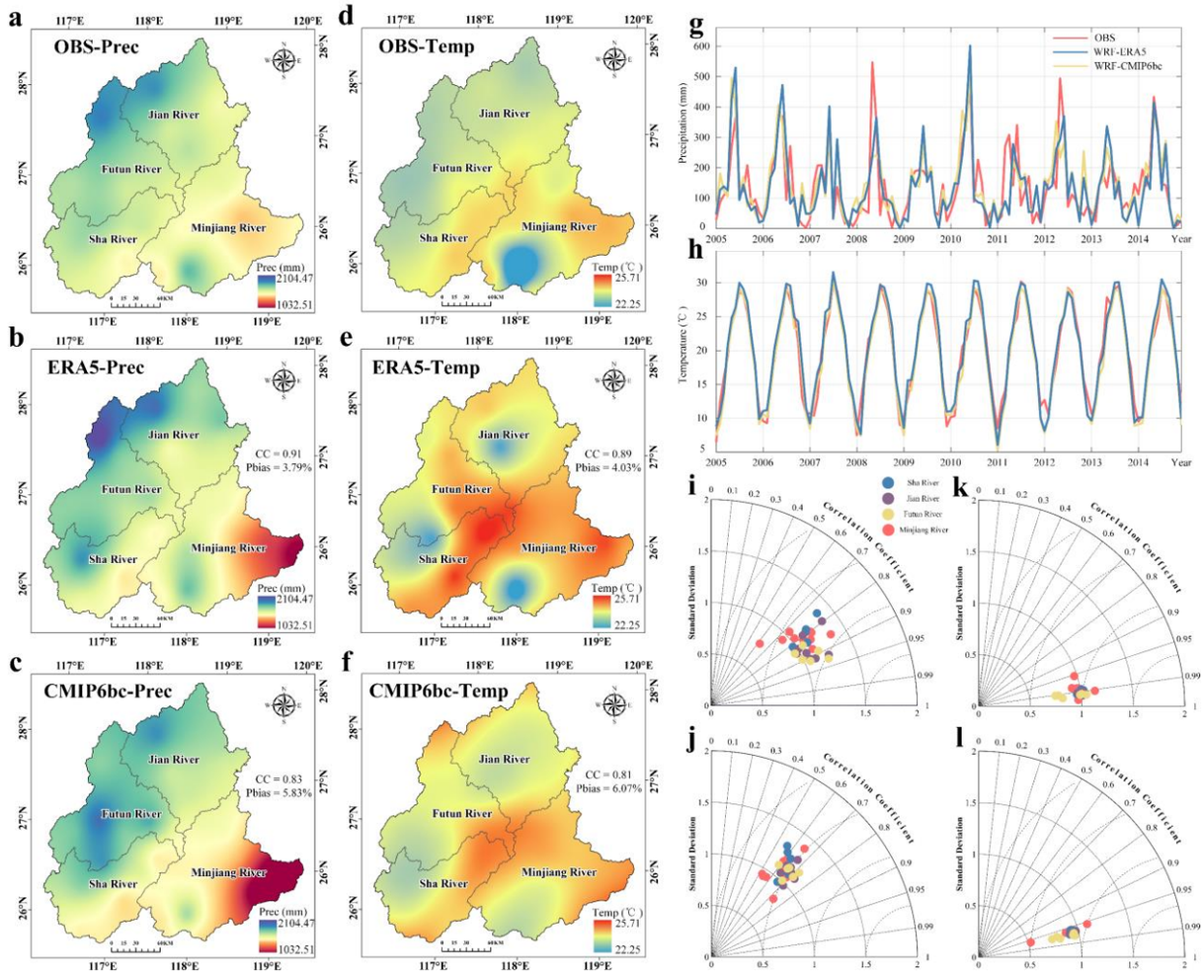

Figure S1. Evaluation of WRF-simulated precipitation and temperature over the MRB (2005-2014). spatial patterns of precipitation (a–c), temperature (d–f). Temporal evolution of precipitation (g) and temperature (h). Panels (i–l) present sub-basin comparisons of precipitation and temperature from ERA5 (i, k) and CMIP6bc (j, l).

iii. How were the spatial results constructed from the observed data at 30 stations?

-Answer: Thank you for your question. We have provided a detailed description in lines 18-24 of the supplementary file.

Table S3 presents the specific information for each station, Table S4 and S5 show the simulated temperature results from CMIP6bc and ERA5, and Table S6 and S7 display the simulated precipitation results. The spatial patterns of precipitation and temperature (Figures S1 a–f) are constructed by performing spline interpolation on the observed data from the 30 stations in the

MRB using Arc Geographic Information System (ArcGIS). To eliminate the interpolation errors, we extracted the nearest WRF grid points for each meteorological station and compared them by plotting a Taylor diagram (Figures S1 i-l).

iv. Please define in the manuscript what CC and PBIAS mean, and clarify whether they represent averages across all grid cells.

-Answer: Thank you for your comment. We have added the details in Table S8 of the supplementary file.

Table S8 Definition of evaluation criteria.

Metric	Formula	Optimal value	Range
CC	$CC = \frac{\sum_{i=1}^{n}(O_i - \overline{O_i})(M_i - \overline{M_i})}{\sqrt{\sum_{i=1}^{n}(O_i - \overline{O_i})^2}\sqrt{\sum_{i=1}^{n}(M_i - \overline{M_i})^2}}$	1	(0, 1)
PBIAS	$PBIAS = \sum_{i=1}^{n} \frac{M_i - O_i}{O_i}$	0	(-∞, +∞)
RMSE	$RMSE = \sqrt{\frac{1}{n}\sum_{i=1}^{n}(M_i - O_i)}$	0	(0, +∞)
STD	$STD = \sqrt{\frac{1}{n}\sum_{i=1}^{n}(O_i - \bar{O})^2}$	0	(0, +∞)

Notes: Where O_i presents meteorological data at the i station, M_i presents data at the WRF grid point closest to the i station, n is the numbers of stations.

v. What are subplots a-f in Figure S1 based on? The mean value per grid over the 10-year historic period? Please add necessary details on what you are comparing.

-Answer: Thank you for your comment. We have provided the details in lines 20-24 of the supplementary file. The spatial patterns of precipitation and temperature (Figures S1 a–f) are constructed by performing spline interpolation on the observed data from the 30 stations in the MRB using Arc Geographic Information System (ArcGIS). It represents the interpolated annual mean values at each meteorological station and the nearest WRF grid point over the 10-year historical period.

vi. Is there also an explanation on those misestimated CMIP6bc temperatures? And why are the results particularly worse in the downstream sub-basin of the MRB?

-Answer: Thank you for your question. Thank you for your question. We have provided an

explanation in lines 43-49 of the supplementary file.

High-altitude areas typically experience stronger radiation effects, especially in mountainous regions with thinner atmospheres. The WRF model may have errors in simulating radiation transfer, leading to temperatures in high-altitude areas being lower than actual conditions (Varga et al., 2020). In addition, the downstream area of the MRB is an urban agglomeration, where urban areas typically experience stronger radiation and heat accumulation effects. These effects may not be fully accounted for in the model, leading to simulated temperatures being higher than actual conditions (Chen et al., 2025).

b. I suggest to swap Sect. 2.3 and 2.4, since you first run the model and then extract CCEs from the model results.

-Answer: Thank you for your suggestion. We have followed your advice and swapped the order of these two sections in the revised manuscript.

i. When identifying the CCE events, did you do it independently for each grid? What are the spatiotemporal definitions of CCEs?

-Answer: Thank you for your question. In response to your inquiry, indeed, when identifying compound climate extremes (CCEs), we performed calculations independently for each grid point. Specifically, we sorted the precipitation and temperature data for each grid point over a 40-year period and defined extreme events based on the 10th and 90th percentiles. The methodology we used is based on the approach outlined by Wang et al. (2024), and the calculations are conducted using independent thresholds for each grid point, without considering co-occurrence of extreme events across multiple grid points. As for the issue of spatially compound disasters, I will address that in my response to the next question.

ii. Did you consider the spatially compound events, i.e. the same CCE event occur at multiple locations simultaneously? If not, please discuss if the proposed approach may double count CCEs and how does this affect your conclusion.

-Answer: Thank you for your question. You've raised a very important point, and we fully understand your concern about whether the simultaneous occurrence of the same compound climate extreme event (CCE) across multiple grid points might lead to double counting, potentially affecting the reliability of the results. In response, we would like to clarify that when calculating

the compound extreme indices, we perform the calculations independently for each grid point. For example, in Figure 3, subplots a-j show the annual mean spatial distribution of each type of CCE for each grid point over the 40-year period, rather than the total sum. Therefore, even if the same event occurs at multiple grid points simultaneously, this will not lead to double counting (For example, even if the same CCE occurs on the same day at two grid points, it will still be counted as one day after averaging.). Similarly, for subplots k-o, the time series variations are averaged across the grid points, representing the mean values of the entire basin, not the total sum, so there is no issue of double counting in these results either. Nevertheless, we appreciate the insightful nature of your comment. Spatially compound events are a more complex concept, and we intend to conduct separate analyses for such cases in future studies.

c.Please include the results of your sensitivity experiments (L130) in the supplementary materials.

-Answer: Thank you for your suggestion. We have added the results of our sensitivity experiments in Supplementary Results S2, as well as in Tables S9 and S10, and Figures S2, S3, and S4.

Result S2 WRF parametrization scheme sensitivity experiments.

In our previous study, we conducted a detailed sensitivity analysis and optimization of parameterization schemes specifically for the MRB (Lin et al., 2023). We focused on two schemes that have the most significant impact on precipitation: microphysics and cumulus convection. By cross-combining these schemes, we developed 16 combinations (as shown in Table S9) and assessed their performance in simulating precipitation across different magnitudes. Through a comprehensive evaluation of the temporal (Figure S2 and Figure S3) and spatial (Figure S4 and Table S10) characteristics, we determined that the 9th configuration (Lin and NT) is the most suitable for simulating extreme precipitation events in the MRB. As a result, this configuration was adopted in the present study to ensure the most accurate simulation of extreme precipitation events in this region.

Table S9 Parameterization scheme combinations design.

Combinations	Microphysics scheme (MP)	Cumulus scheme (CU)
EXP1	WSM6	Betts-Miller-Janjic (BMJ)
EXP2	WSM6	Betts-Miller-Janjic (BMJ)
EXP3	WSM6	Betts-Miller-Janjic (BMJ)
EXP4	WSM6	Betts-Miller-Janjic (BMJ)
EXP5	WDM6	Kain-Fritsch (KF)
EXP6	WDM6	Kain-Fritsch (KF)
EXP7	WDM6	Kain-Fritsch (KF)
EXP8	WDM6	Kain-Fritsch (KF)
EXP9	Purdue Lin (Lin)	New Tiedtke (NT)
EXP10	Purdue Lin (Lin)	New Tiedtke (NT)
EXP11	Purdue Lin (Lin)	New Tiedtke (NT)
EXP12	Purdue Lin (Lin)	New Tiedtke (NT)
EXP13	Thompson	Grell-Devenyi (GD)
EXP14	Thompson	Grell-Devenyi (GD)
EXP15	Thompson	Grell-Devenyi (GD)
EXP16	Thompson	Grell-Devenyi (GD)

Table S10 Evaluation metrics for total accumulated precipitation

Combination	TS (light)	TS (moderate)	TS (heavy)	TS (torrential)	$\overline{TS}$	$\overline{POD}$	$\overline{FAR}$
EXP1	0.22	0.11	0.07	0.15	0.14	0.24	0.71
EXP2	0.22	0.10	0.14	0.08	0.14	0.24	0.69
EXP3	0.24	0.11	0.09	0.16	0.15	0.27	0.66
EXP4	0.22	0.05	0.14	0.14	0.14	0.25	0.70
EXP5	0.14	0.07	0.07	0.11	0.10	0.16	0.71
EXP6	0.12	0.09	0.09	0.07	0.09	0.15	0.74
EXP7	0.18	0.09	0.10	0.12	0.12	0.20	0.64
EXP8	0.16	0.09	0.11	0.14	0.12	0.19	0.68
EXP9	0.26	0.11	0.12	0.16	0.16	0.29	0.66
EXP10	0.22	0.10	0.11	0.11	0.14	0.24	0.74
EXP11	0.24	0.12	0.13	0.14	0.16	0.23	0.55
EXP12	0.25	0.10	0.10	0.13	0.15	0.24	0.71
EXP13	0.22	0.10	0.07	0.11	0.12	0.21	0.67
EXP14	0.21	0.08	0.08	0.06	0.11	0.20	0.74
EXP15	0.24	0.09	0.10	0.13	0.14	0.25	0.70
EXP16	0.24	0.12	0.13	0.12	0.15	0.26	0.67

Note: TS (light rain, moderate rain, heavy rain, torrential rain) refers to the average of daily 24-hour accumulated precipitation. $\overline{TS}$, $\overline{POD}$ and $\overline{FAR}$ represent the average values of the scores for the four precipitation levels.

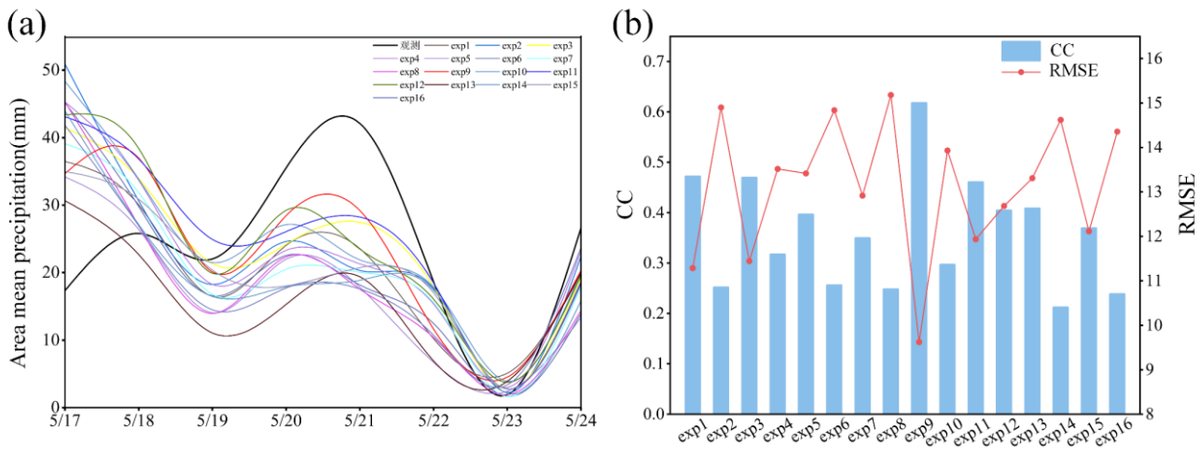

Figure S2. Time series of observations and WRF simulation.

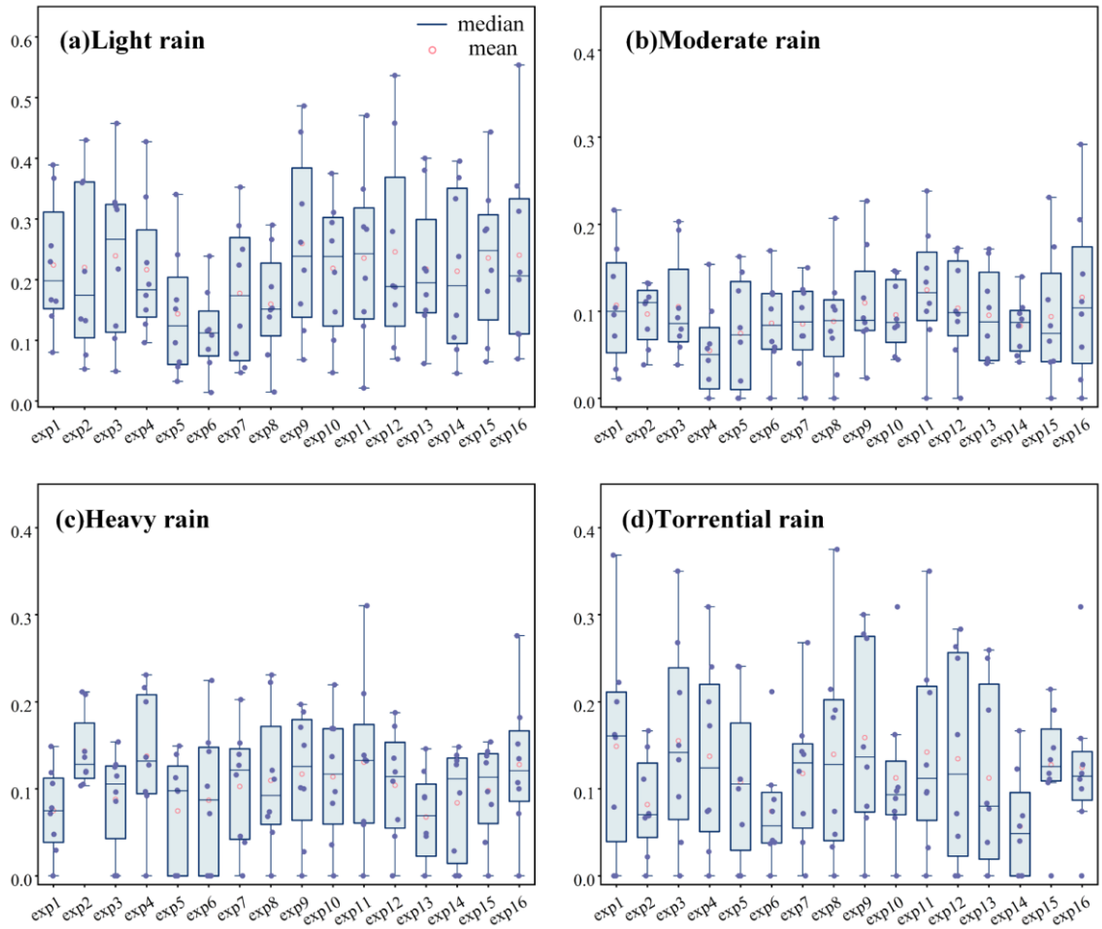

Figure S3. Box plot of TS scores for 24-hour accumulated precipitation simulated by WRF.

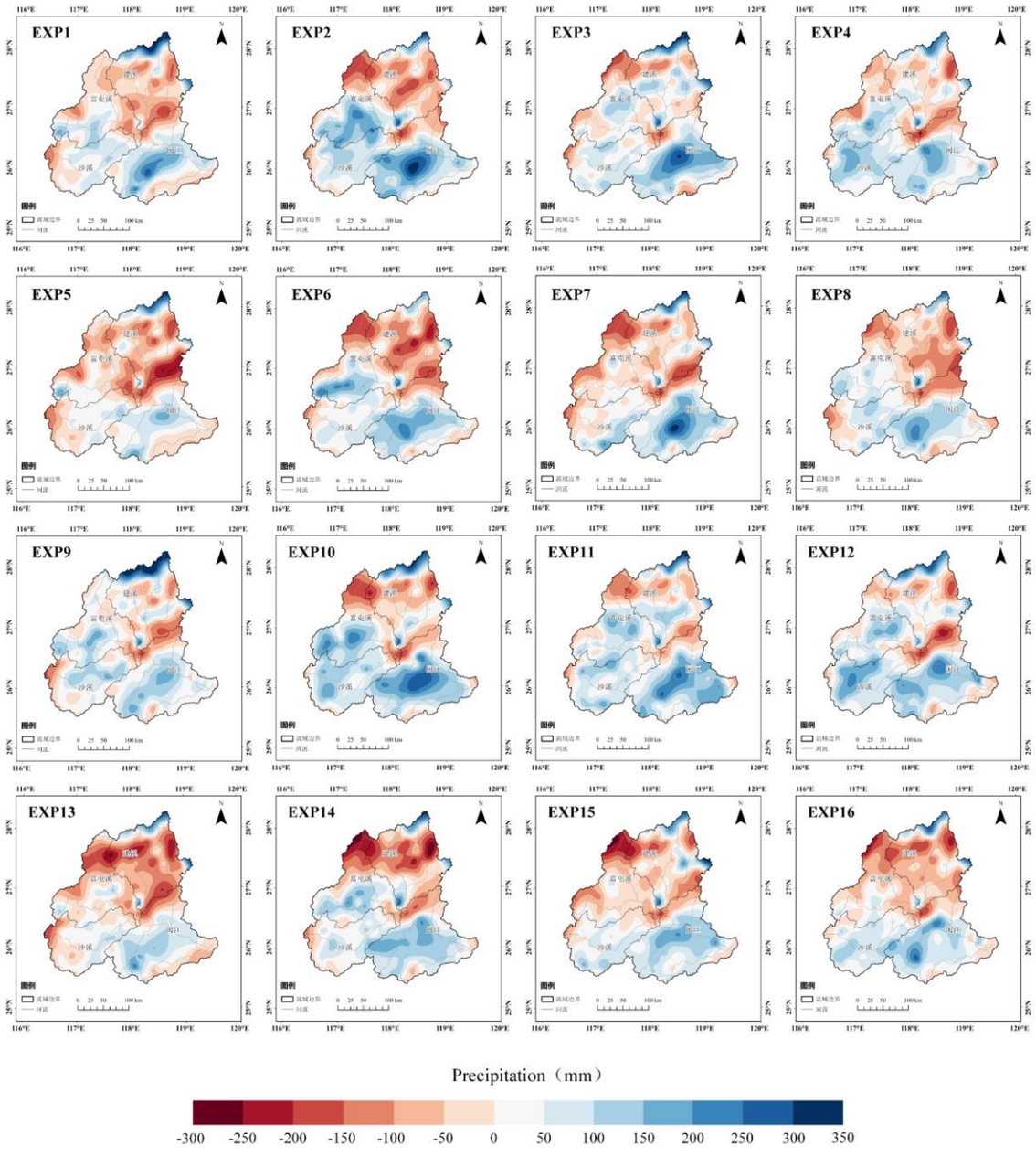

Figure S4. Spatial distribution of biases of total accumulated precipitation from WRF parametrization scheme sensitivity experiments.

d.While Sect. 2.4.2 introduces the GAMLSS model, it lacks the detail on how WRF results are used in this model. The authors may include suitable examples when explaining the proposed approach. For example, how are the daily temperature and precipitation or the identified CCEs used in the model?

-Answer: Thank you for your suggestion. We have provided detailed explanations for these two issues in lines 125-131 and 248-254 of the revised manuscript.

To address these research gaps, this study adopts a high-resolution approach by integrating the WRF model with GAMLSS. We first perform dynamical downscaling using the WRF model to refine the bias-corrected Coupled Model Intercomparison Project Phase 6 (CMIP6bc) data (1.25° × 1.25°) to a 3 km resolution. Based on these high-resolution WRF outputs, CCEs are then identified and used as input for the GAMLSS framework to analyze their non-stationary characteristics. This methodology overcomes the limitations of traditional coarse-resolution models and addresses the shortcomings of stationary assumptions in CCE analysis.

We conduct calculations independently for each grid point, applying thresholds specific to each point. Specifically, for interannual variation, we sort the precipitation and temperature data over a 40-year period and determine the thresholds based on the 10th and 90th percentiles to identify CCEs. For seasonal variations, we separately extract the precipitation and temperature data for the summer (JJA) and winter (DJF) seasons, applying the same sorting method to calculate the respective thresholds, thus analyzing the distribution characteristics of CCEs for each season.

e.L158-159: "we fit non-stationary GAMLSS models with two parameters (mean, variance) and four parameters (mean, variance, skewness, kurtosis) at each grid point, selecting the optimal model for subsequent analysis." What is the difference between the mean and variance in the first mention (two parameters) and in the following (four parameters)? And how are the changes between the current and future CCE frequency estimated and in what unit/form?

-Answer: Thank you for your question. We have provided a detailed explanation in lines 280-289 of the revised manuscript.

In the GAMLSS model, time (year) is used as the independent variable (x), and the number of days per year for each type of CCE is treated as the dependent variable (y), thereby enabling the calculation of the non-stationary characteristics of each CCE. We employ two types of GAMLSS

models to capture potential changes in the distribution of meteorological variables. The first is the traditional two-parameter location–scale model (mean μ and variance σ), which assumes a fixed distributional shape. The second is a more flexible four-parameter location–scale–shape model (mean μ, variance σ, skewness ν, and kurtosis τ), allowing the distributional shape to evolve over time. These extended models retain the mean and variance parameters while incorporating two additional shape parameters to capture asymmetry and tail behavior. We assess the models by comparing their goodness of fit and select the one that best represents the data distribution for subsequent analyses. Regarding the calculation of stationarity, we consider the CCEs to be stationary if both the mean and variance remain stable. If either the mean or variance shows significant variation, the CCEs are considered non-stationary.

Additionally, skewness and kurtosis are unitless statistics that measure the asymmetry and tail thickness of the data distribution, respectively. The unit of frequency change is days per decade, and it was calculated by using linear regression based on annual data to estimate the trend of frequency change.

6.Please describe in the methodology how metrics such as annual event distribution, seasonal variations, and non-stationary characteristics were calculated.

-Answer: Thank you for your question. We have provided a detailed explanation of these two issues in lines 248-254 and 287-289 of the revised manuscript.

We conduct calculations independently for each grid point, applying thresholds specific to each point. Specifically, for interannual variation, we sort the precipitation and temperature data over a 40-year period and determine the thresholds based on the 10th and 90th percentiles to identify CCEs. For seasonal variations, we separately extract the precipitation and temperature data for the summer (JJA) and winter (DJF) seasons, applying the same sorting method to calculate the respective thresholds, thus analyzing the distribution characteristics of CCEs for each season.

Regarding the calculation of stationarity, we consider the CCEs to be stationary if both the mean and variance remain stable. If either the mean or variance shows significant variation, the CCEs are considered non-stationary.

7.In Fig. 3 (a-j), do the annual spatial values refer to the mean yearly event number over 2025-2065? What does d/10a mean?

-Answer: Thank you for your question. We apologize for the previous lack of clarity in our description. In Figure 3 (a-j), the annual spatial values represent the mean yearly event number over the period 2025-2065. Regarding the term "d/10a," we have revised it to ‘days per decade’ to ensure clearer understanding.

8.When looking at the temporal changes in CCEs (Fig. 3 k-o), it is interesting to see the projections for two SSPs sometimes show a completely different year-to-year trend. For example, for hot-dry events, the value in blue increases from 2032 to 2033 while the red one decreases. There are also similar discrepancies for different years and different compound events. Is there an explanation for this?

-Answer: Thank you for pointing out this important issue. The inconsistency, or even opposite trends, of extreme events in some regions under the SSP2-4.5 and SSP5-8.5 pathways in climate simulations is reasonable and expected. This is mainly due to the dominant role of internal climate variability at the regional scale. Although the greenhouse gas forcing in SSP5-8.5 is stronger, the global warming and atmospheric circulation responses (such as changes in jet stream positions or shifts in storm tracks) caused by it differ spatially from those in SSP2-4.5. These differences interact in complex ways with decadal-scale internal oscillations, such as the Pacific Decadal Oscillation (PDO) or the Atlantic Multidecadal Oscillation (AMO). During specific periods and in certain regions, these strong natural variability signals may temporarily mask or even reverse the long-term trends driven by external forcing, leading to different short-term evolution paths under the two scenarios. Additionally, similar cases have been observed in previous studies (Figure 5 (Wu et al., 2023); Figure 7 (Ren et al., 2023); Figure 2 (Fang et al., 2025)), demonstrating that short-term variability under different emission scenarios is quite common.

9.Similar to my earlier comment, if you did not consider the same CCE occurring across cells. Be careful with drawing conclusions from the averaged days as you may double count some events.

-Answer: Thank you very much for your question. The response to this issue is the same as for question 5. b. II. We perform the calculations independently for each grid point. For example, in Figure 3, subplots a-j show the annual mean spatial distribution of each type of CCE for each grid

point over the 40-year period, rather than the total sum. Therefore, even if the same event occurs at multiple grid points simultaneously, this will not lead to double counting (For example, even if the same CCE occurs on the same day at two grid points, it will still be counted as one day after averaging.). Similarly, for subplots k-o, the time series variations are averaged across the grid points, representing the mean values of the entire basin, not the total sum, so there is no issue of double counting in these results either. Nevertheless, we appreciate the insightful nature of your comment. Spatially compound events are a more complex concept, and we intend to conduct separate analyses for such cases in future studies.

10.For showing the seasonal variations, I was wondering would it be better to compare the event number/frequency between different seasons for a given CCE, instead of presenting results for all four CCEs for a given season.

-Answer: Thank you for your feedback. We have changed the presentation as per your suggestion in lines 352-357 of the revised manuscript.

11.How were the return periods calculated?

-Answer: Thank you for your question. In this study, the calculation of return periods is based on the threshold exceedance method, which fundamentally links the return period to the frequency of extreme events. Specifically, we extracted all extreme events from the historical data that exceeded the predetermined threshold and constructed a sequence of their "frequency (days per year)." By analyzing this frequency and fitting the optimal distribution (Gao et al., 2018), we calculated the "frequency for a 10-year return period" (for example, X days per decade). This means that a "10-year return period event" refers to the frequency of such an event occurring.

12.I find the discussion section relatively weak, as certain findings lack sufficient reasoning or possible explanations. Furthermore, the biases in precipitation simulation are considered as a key limitation of this study. How big are the influences of these biases on your findings? Do you consider using bias-correction methods in the future studies?

-Answer: Thank you for your comment. We have enriched our discussion section and have divided our results into four points for a more detailed discussion.

4 Discussion

Although earlier research has emphasized the necessity of analyzing extreme events under non-

stationary conditions (Cheng et al, 2014; Byun and Hamlet, 2020; Liu et al., 2024), the evolution of CCEs within a non-stationary climate remains lacking. Our study develops an innovative non-stationary framework integrating WRF-based dynamical downscaling with GAMLSS to reassess future recurrence frequency of CCEs. The results indicate that traditional stationary models systematically underestimate the frequency of CCEs, highlighting the critical importance of incorporating time-varying risk assessments to avoid misleading projections and to inform robust climate adaptation strategies (Abdelmoaty and Papalexiou, 2023). This innovative framework enables regional-scale reassessment of CCEs which is transferable to other regions.

4.1 Dominance of hot extremes and temperature-driven shifts

The projected increase in CCEs, particularly under SSP5-8.5, aligns with global trends of intensifying hydroclimatic risks under continued warming (Asadieh and Krakauer, 2017; Zhang et al., 2021; Shu et al., 2024). Our findings indicate that hot-dry extremes dominate both spatially and temporally, increasing at 2.26 days per decade in summer under SSP5-8.5, while cold extremes decline. This pattern is consistent with studies highlighting the rising prevalence of hot-stagnation and hot-dry extremes in East Asia (Yin et al., 2025). The reversal between hot and cold extremes has been robustly linked to enhanced radiative forcing from anthropogenic greenhouse gas emissions (Samset et al., 2018; Kramer et al., 2021). Our analysis further reveals that temperature—not precipitation—is the primary driver of CCE changes in the MRB, as evidenced by the strong warming trend (0.46°C per decade under SSP5-8.5) alongside relatively stable precipitation (Supplement Figure S2). This supports the hypothesis that thermodynamic effects, rather than dynamic ones, dominate mean-state changes in extremes (Horton et al., 2016; Van Der Wiel and Bintanja, 2021).

4.2 Non-stationarity: mean shifts outpace variability

A key advance of this study is the explicit detection of non-stationary characteristics in CCEs, which has been largely overlooked in prior compound event analyses. We find that under SSP5-8.5, 95.20% of grid cells exhibit non-stationarity, predominantly driven by changes in the Mn rather than Var, accounting for 80.81% of the transitions. This suggests that climate warming amplifies extremes primarily through shifts in baseline intensity—a thermodynamic effect—rather than through increased temporal variability. Similar findings have been reported at global scales, where mean

warming dominates changes in extreme temperature distributions (Patel et al., 2024; Nordling et al., 2025). The spatial concentration of Mn-driven non-stationarity in downstream MRB and the Shaxi River Basin may reflect localized warming amplification due to urban heat islands or land-atmosphere feedbacks, a phenomenon noted in other subtropical regions (Gao et al., 2018; Wu et al., 2020).

4.3 Frequency of recurrence systematically underestimated by stationary model

Our comparison between stationary and non-stationary model indicates that the latter captures a significant increase in recurrence risks, particularly for 100-year CCEs, which are projected to rise by 3.12 days per decade under the SSP5-8.5 scenario. Stationary model systematically underestimates recurrence frequency after 2045, and the stronger non-stationary response of 100-year events highlights the heightened vulnerability of high-impact, low-probability extremes. Additionally, the west-to-east gradient in recurrence frequency, with hotspots in the Shaxi River Basin, may be attributed to topographic and land-surface heterogeneity, which modulate local hydroclimatic responses (Zheng et al., 2023). Previous studies have similarly shown that conventional extreme value models fail to capture the escalating severity of extreme events under climate change. Singh et al. (2021) demonstrated that under climate change, precipitation and temperature exhibit a non-stationary dependent structure, and treating them independently can substantially underestimate the occurrence of compound extremes. Feng et al. (2020) compared the recurrence probabilities of floods under stationary and non-stationary conditions and found that, under non-stationary conditions, the annual variability of floods is significantly greater. Xu et al. (2025) evaluated changes in global marine heatwaves and found that stationary models significantly underestimate their frequency, intensity, and duration. In summary, these studies collectively highlight that accounting for non-stationarity is crucial for accurately assessing various extreme events.

4.4 Methodological limitations

Our integrated 'bias-corrected CMIP6–WRF dynamical downscaling–GAMLSS' framework represents a significant methodological advancement over the direct use of purely statistical downscaling for projecting CCEs. By resolving mesoscale circulations and explicitly simulating convective processes, our approach more faithfully captures the fine-scale spatiotemporal

heterogeneity of precipitation and temperature fields in complex terrain, a capability that statistical methods, reliant on historically derived statistical relationships, fundamentally lack (Gutmann et al., 2012; Rahimi et al., 2024). Nevertheless, certain limitations persist. Even at convection-permitting resolution (3 km), the WRF model exhibits systematic biases in simulating orographic precipitation, a well-documented challenge often stemming from uncertainties in microphysical parameterization schemes and the representation of land-atmosphere energy and moisture exchanges over mountainous regions (Talbot et al., 2012; Zhang et al., 2025). Furthermore, while statistically robust, our current non-stationary GAMLSS framework employs time merely as a proxy covariate for climate change. This approach effectively detects and projects temporal trends in risk but falls short of elucidating the underlying physical drivers, such as the specific roles of evolving large-scale circulation patterns or soil moisture-atmosphere feedbacks. To overcome these constraints and solidify the physical foundations of our projections, future work should focus on three promising avenues: first, explicitly embedding physical drivers like atmospheric circulation indices, antecedent soil moisture, or global mean temperature as covariates within the GAMLSS to establish a clearer causal chain from forcing to statistical response (Zeng et al., 2024; Ma et al., 2025); second, leveraging machine learning, such as convolutional neural networks, for the statistical post-processing of WRF outputs to correct systematic biases, or developing hybrid physics-informed machine learning models as a complementary approach to dynamical downscaling (Yin et al., 2021; Xie et al., 2023); and third, employ multi-RCMs ensemble forecasts to comprehensively address and minimize the uncertainties inherent in the downscaling process, thereby enhancing the robustness and reliability.

Minor Comments:

1.L29: Write out 3.55d/10a.

-Answer: Thank you for your valuable comment. We apologize for the incorrect expression of "3.55 d/10a." Following your suggestion, we have changed all such expressions to "days per decade" in the revised version to ensure clarity and consistency.

2.L32: Define stationarity.

-Answer: Thank you for your suggestion. We have added further clarification on this concept in lines 105-108 of the revised manuscript.

Additionally, traditional extreme event analyses rely on stationarity assumptions (when analyzing time series data, it is assumed that the statistical properties of the series remain constant over time), presuming that the probability and distributional parameters of climate variables are constant (Sun et al., 2018; Nerantzaki et al., 2023).

3.L55: considering rephrasing the sentence into Therefore, traditional models fail to capture the non-stationary changes in these extreme events.

-Answer: Thank you for your suggestion. We have made revisions in lines 110-112 of the revised manuscript.

Therefore, traditional models fail to capture the non-stationary (the statistical properties of a time series change over time and do not remain constant) changes in these extreme events.

4.In L71, the WRF model appears rather abruptly. Please introduce its relation with the RCMs.

-Answer: Thank you for your suggestion. We have added additional information in lines 77-104 of the revised manuscript.

While large-scale studies play a crucial role in advancing our understanding of global climate change and extreme events, their practical relevance for disaster risk management and adaptation strategies in medium- and small-scale regions is relatively limited due to their lower spatial and temporal resolution. To overcome this constraint, dynamical downscaling, which utilizes nested high-resolution regional climate models (RCMs), provides a critical technical pathway to investigate climate response mechanisms at fine-scales (Tapiador et al., 2020; Rahimi et al., 2024). Compared to Global Climate Models (GCMs), RCMs offer higher spatial resolution, allowing for more precise simulations of local climate effects induced by topography, such as local convective precipitation, orographic effects, and regional climate heterogeneity (Gilbert et al., 2025). In regions with complex terrain, RCMs are particularly effective at capturing spatial variations of climate variables, such as the differences in wind patterns, precipitation, and their distribution caused by topography in mountainous or basin areas (Imran and Evans, 2025). For example, Byun et al. (2023) assessed the ability of RCMs and GCMs to simulate storm tracks in East Asia, revealing that RCMs are better able to capture high-resolution topography, thereby reducing the biases found in GCMs. Lin et al. (2022) showed that RCMs driven by ERA-Interim reanalysis data are capable of capturing small-scale processes, such as orographic effects, and outperform GCMs

in reproducing the large-scale features of the Heat Wave Magnitude Index-daily. Torrez-Rodriguez et al. (2023) also demonstrated that RCMs are better at reproducing the main spatio-temporal characteristics of precipitation in subtropical complex terrain regions. As an advanced convection-permitting RCM, the WRF model significantly enhances the simulation capability for meteorological processes at 1-10 km scales through its fully compressible, non-hydrostatic dynamic core framework (Talbot et al., 2012). This high-resolution simulation capability gives the WRF model a unique advantage in capturing small-scale meteorological phenomena. Zhou et al. (2024) developed a 9 km resolution regional reanalysis dataset covering the Tibetan Plateau based on the WRF model, and demonstrated its superior applicability compared to the fifth generation European Centre for Medium-Range Weather Forecasts Reanalysis (ERA5). Yang et al. (2024) revealed that the WRF model provides better accuracy in simulating snow depth during the cold season in high-elevation regions compared to ERA5-Land.

5.Similarly, in L78, please add how GAMLSS and WRF fit in here. While introducing the objective of this paper, the authors should mention what types of CCEs they are looking into.

-Answer: Thank you for your suggestion. We have added additional information in lines 125-131 of the revised manuscript.

To address these research gaps, this study adopts a high-resolution approach by integrating the WRF model with GAMLSS. We first perform dynamical downscaling using the WRF model to refine the bias-corrected Coupled Model Intercomparison Project Phase 6 (CMIP6bc) data (1.25° × 1.25°) to a 3 km resolution. Based on these high-resolution WRF outputs, CCEs are then identified and used as input for the GAMLSS framework to analyze their non-stationary characteristics. This methodology overcomes the limitations of traditional coarse-resolution models and addresses the shortcomings of stationary assumptions in CCE analysis. By focusing on the Minjiang River Basin (MRB)—a subtropical, monsoon-dominated basin in southeastern China where complex topographic–climatic interactions give rise to high-intensity compound hydroclimatic extremes (Gan et al., 2025; Geng et al., 2024; Wang et al., 2024)—this research aims to examine four types of CCEs: hot-wet (HW), hot-dry (HD), cold-wet (CW), and cold-dry (CD) events.

6.Please add references to support the statement 'complex interactions between topography and climate give rise to high-intensity compound hydroclimatic extremes.' (L81-82).

-Answer: Thank you for your suggestion. We have added additional information in lines 131-136 of the revised manuscript.

By focusing on the Minjiang River Basin (MRB)—a subtropical, monsoon-dominated basin in southeastern China where complex topographic–climatic interactions give rise to high-intensity compound hydroclimatic extremes (Gan et al., 2025; Geng et al., 2024; Wang et al., 2024)—this research aims to examine four types of CCEs: hot-wet (HW), hot-dry (HD), cold-wet (CW), and cold-dry (CD) events.

7.Define non-stationarity detection (L85).

-Answer: Thank you for your suggestion. We have added additional information on this definition in lines 110-112 of the revised manuscript.

Therefore, traditional models fail to capture the non-stationary (the statistical properties of a time series change over time and do not remain constant) changes in these extreme events.

8.L109, write out ERA5 if it is the first use.

-Answer: Thank you for your suggestion. We have made revisions in lines 99-102 of the manuscript.

Zhou et al. (2024) developed a 9 km resolution regional reanalysis dataset covering the Tibetan Plateau based on the WRF model, and demonstrated its superior applicability compared to the fifth generation European Centre for Medium-Range Weather Forecasts Reanalysis (ERA5).

9.Provide the names and associated details of the 18 models used in your dataset.

-Answer: Thank you for your suggestion. We have provided a list of the 18 models used in the bias-corrected CMIP6 dataset (Xu et al., 2021) in the supplementary file as requested.

Table S1 CMIP6 models used in CMIP6bc.

No.	Model	Institution	Approximate grid spacing
1	ACCESS-CM2	Commonwealth Scientific and Industrial Research Organisation (Australia)	1.875° × 1.25°
2	ACCESS-ESM1–5	Commonwealth Scientific and Industrial Research Organisation (Australia)	1.875° × 1.25°
3	CanESM5	Canadian Centre for Climate Modelling and Analysis (Canada)	2.81° × 2.81°
4	BCC-CSM2-MR	Beijing Climate Center (China)	1.125° × 1.125°
5	FGOALS-f3-L	Institute of Atmospheric Physics, Chinese Academy of Sciences (China)	1.25° × 1°
6	FGOALS-g3	Institute of Atmospheric Physics, Chinese Academy of Sciences (China)	2° × 2.25°
7	EC-Earth3	European EC-Earth Consortium (Europe)	0.70° × 0.70°
8	EC-Earth3-Veg	European EC-Earth Consortium (Europe)	0.70° × 0.70°
9	IPSL-CM6A-LR	Institute Pierre Simon Laplace (France)	2.5° × 1.26°
10	AWI-CM-1-1-MR	Alfred Wegener Institute, Helmholtz Centre for Polar and Marine Research (Germany)	0.94° × 0.94°
11	MPI-ESM1-2-HR	Max Planck Institute for Meteorology (Germany)	0.94° × 0.94°
12	MPI-ESM1-2-LR	Max Planck Institute for Meteorology (Germany)	1.875° × 1.875°
13	MIROC6	Japan Agency for Marine-Earth Science and Technology (Japan)	1.41° × 1.41°
14	MRI-ESM2-0	Meteorological Research Institute, Japan Meteorological Agency (Japan)	1.125° × 1.125°
15	NorESM2-LM	Norwegian Climate Center (Norway)	2.5° × 1.875°
16	CESM2	Climate and Global Dynamics Laboratory, National Center for Atmospheric Research (USA)	1.25° × 0.94°
17	CESM2-WACCM	Climate and Global Dynamics Laboratory, National Center for Atmospheric Research (USA)	1.25° × 0.94°
18	GFDL-ESM4	Geophysical Fluid Dynamics Laboratory, National Oceanic and Atmosphere Administration (USA)	1.25° × 1.0°

10.In Fig. 2, please consider using another color for the meteorological stations as they are sometimes hard to tell due to the elevation data.

-Answer: Thank you for your suggestion. We have modified this figure accordingly and use a different color for the meteorological stations in the revised version to avoid confusion with the elevation data (Figure 2).

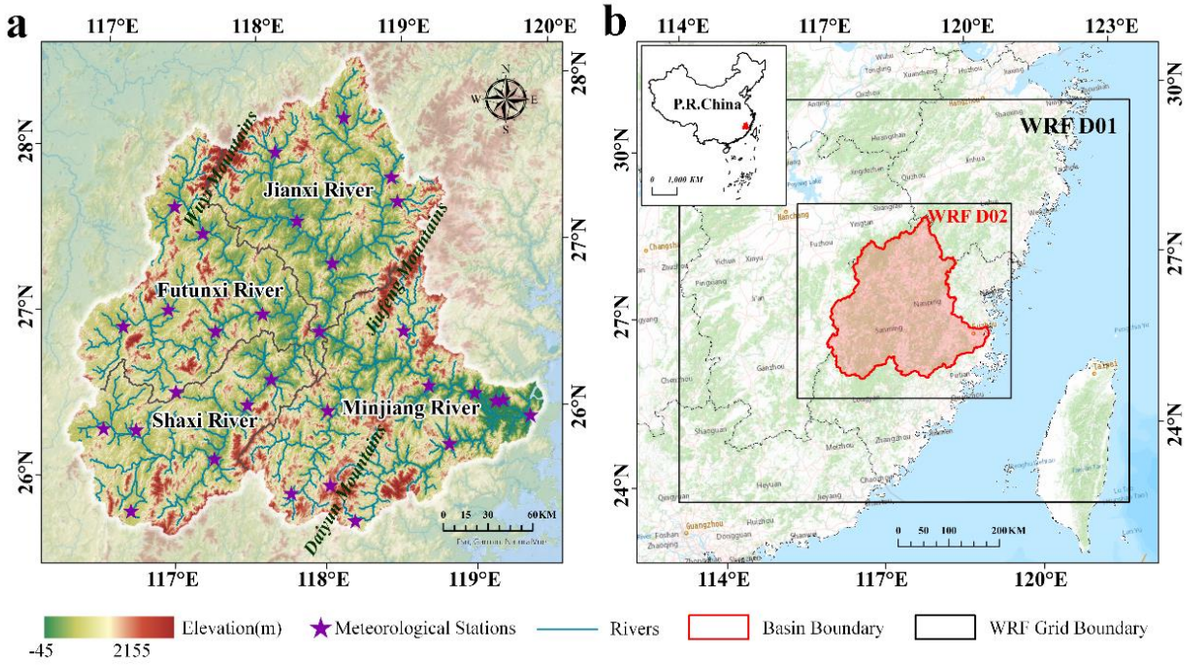

Figure 2. Study area and model configuration. (a) Topographic features of the MRB (m) and (b) Model configuration with 9-km (D01) and 3-km (D02) nested domains (Zhang et al., 2025). Basemap source: © Esri, https://services.arcgisonline.com

11.When referring to the figures, please use Fig. instead of Figure to make sure it is consistent with the captions.

-Answer: Thank you for your suggestion. We have standardized both the figure titles and references to 'figure' in the revised version.

References

Asadieh, B., Krakauer, N.Y., 2017. Global change in streamflow extremes under climate change over the 21st century. Hydrol. Earth Syst. Sci. 21, 5863–5874. https://doi.org/10.5194/hess-21-5863-2017

Byun, K., Hamlet, A.F., 2020. A risk-based analytical framework for quantifying non-stationary flood risks and establishing infrastructure design standards in a changing environment. J. Hydrol. 584, 124575. https://doi.org/10.1016/j.jhydrol.2020.124575

Byun, U., Chang, E., Kim, J., Ahn, J., Cha, D., Min, S., Byun, Y., 2023. Investigation of Added Value in Regional Climate Models for East Asian Storm Track Analysis. JGR Atmospheres 128, e2023JD039167. https://doi.org/10.1029/2023JD039167

Chen, G., Mei, S.-J., Hang, J., Li, Q., Wang, X., 2025. URANS simulations of urban microclimates: Validated by scaled outdoor experiments. Building Environ. 272, 112691. https://doi.org/10.1016/j.buildenv.2025.112691

Cheng, L., AghaKouchak, A., Gilleland, E., Katz, R.W., 2014. Non-stationary extreme value analysis in a changing climate. Climatic Change 127, 353–369. https://doi.org/10.1007/s10584-014-1254-5

Fang, P., Wang, T., Yang, D., Tang, L., Yang, Y., 2025. Substantial increases in compound climate extremes and associated socio-economic exposure across China under future climate change. npj Clim. Atmos. Sci. 8, 17. https://doi.org/10.1038/s41612-025-00910-7

Feng, Y., Shi, P., Qu, S., Mou, S., Chen, C., Dong, F., 2020. Nonstationary flood coincidence risk analysis using time-varying copula functions. Sci. Rep. 10, 3395. https://doi.org/10.1038/s41598-020-60264-3

Gan, B., Liu, M., Cui, H., Chen, X., Chen, Y., Gao, L., Deng, H., 2025. Spatiotemporal patterns and propagation of meteorological and hydrological drought in a humid basin of Southeast China. Sci. Rep. 15, 31720. https://doi.org/10.1038/s41598-025-17005-1

Gao, L., Huang, J., Chen, X., Chen, Y., Liu, M., 2018. Contributions of natural climate changes and human activities to the trend of extreme precipitation. Atmos. Res. 205, 60–69. https://doi.org/10.1016/j.atmosres.2018.02.006

Geng, K., Chen, X., Zheng, M., Gao, Y., Gu, Z., Yao, H., 2024. The influence of human activities

on rainfall-runoff relationships at different time scales in the Minjiang River Basin. Theor. Appl. Climatol. 155, 8435–8454. https://doi.org/10.1007/s00704-024-05124-0

Gilbert, E., Pishniak, D., Torres, J.A., Orr, A., Maclennan, M., Wever, N., Verro, K., 2025. Extreme precipitation associated with atmospheric rivers over West Antarctic ice shelves: insights from kilometre-scale regional climate modelling. The Cryosphere 19, 597–618. https://doi.org/10.5194/tc-19-597-2025

Gutmann, E.D., Rasmussen, R.M., Liu, C., Ikeda, K., Gochis, D.J., Clark, M.P., Dudhia, J., Thompson, G., 2012. A Comparison of Statistical and Dynamical Downscaling of Winter Precipitation over Complex Terrain. J. Clim. 25, 262–281. https://doi.org/10.1175/2011JCLI4109.1

Horton, R.M., Mankin, J.S., Lesk, C., Coffel, E., Raymond, C., 2016. A Review of Recent Advances in Research on Extreme Heat Events. Curr. Clim. Change Rep. 2, 242–259. https://doi.org/10.1007/s40641-016-0042-x

Huang, Y., Xue, M., Hu, X., Martin, E., Novoa, H.M., McPherson, R.A., Liu, C., Chen, M., Hong, Y., Perez, A., Morales, I.Y., Ticona Jara, J.L., Flores Luna, A.J., 2024. Increasing frequency and precipitation intensity of convective storms in the Peruvian Central Andes: Projections from convection-permitting regional climate simulations. Quart. J Royal. Meteoro. Soc. 150, 4371–4390. https://doi.org/10.1002/qj.4820

Jamal, K., Li, X., Chen, Y., Rizwan, M., Khan, M.A., Syed, Z., Mahmood, P., 2023. Bias correction and projection of temperature over the altitudes of the Upper Indus Basin under CMIP6 climate scenarios from 1985 to 2100. J. Water Clim. Change 14, 2490–2514. https://doi.org/10.2166/wcc.2023.180

Kramer, R.J., He, H., Soden, B.J., Oreopoulos, L., Myhre, G., Forster, P.M., Smith, C.J., 2021. Observational Evidence of Increasing Global Radiative Forcing. Geophys. Res. Lett. 48, e2020GL091585. https://doi.org/10.1029/2020GL091585

Lei, X., Gao, L., Ma, M., Wei, J., Xu, L., Wang, L., Lin, H., 2021. Does non-stationarity of extreme precipitation exist in the Poyang Lake Basin of China? J. Hydrol.: Reg. Stud. 37, 100920. https://doi.org/10.1016/j.ejrh.2021.100920

Lin, C., Kjellström, E., Wilcke, R.A.I., Chen, D., 2022a. Present and future European heat wave

magnitudes: climatologies, trends, and their associated uncertainties in GCM-RCM model chains. Earth Syst. Dynam. 13, 1197–1214. https://doi.org/10.5194/esd-13-1197-2022

Liu, Y., Chen, J., Xiong, L., Xu, C.-Y., 2024. Integrating heterogeneous information for modeling non-stationarity of extreme precipitation in the Yangtze River Basin. J. Hydrol. 645, 132159. https://doi.org/10.1016/j.jhydrol.2024.132159

Ma, L., Hu, S., Zhou, B., Peng, J., Li, D., 2025. Novel dynamical indices for the variations of the South Asia high in a warming climate. Atmos. Res. 315, 107901. https://doi.org/10.1016/j.atmosres.2024.107901

Nerantzaki, S.D., Papalexiou, S.M., Rajulapati, C.R., Clark, M.P., 2023. Nonstationarity in High and Low-Temperature Extremes: Insights From a Global Observational Data Set by Merging Extreme-Value Methods. Earth's Future 11, e2023EF003506. https://doi.org/10.1029/2023EF003506

Nordling, K., Fahrenbach, N.L.S., Samset, B.H., 2025. Climate variability can outweigh the influence of climate mean changes for extreme precipitation under global warming. Atmos. Chem. Phys. 25, 1659–1684. https://doi.org/10.5194/acp-25-1659-2025

Patel, R.N., Bonan, D.B., Schneider, T., 2024. Changes in the Frequency of Observed Temperature Extremes Largely Driven by a Distribution Shift. Geophys. Res. Lett. 51, e2024GL110707. https://doi.org/10.1029/2024GL110707

Rahimi, S., Huang, L., Norris, J., Hall, A., Goldenson, N., Risser, M., Feldman, D.R., Lebo, Z.J., Dennis, E., Thackeray, C., 2024. Understanding the Cascade: Removing GCM Biases Improves Dynamically Downscaled Climate Projections. Geophys. Res. Lett. 51, e2023GL106264. https://doi.org/10.1029/2023GL106264

Ren, J., Huang, G., Zhou, X., Li, Y., 2023. Downscaled compound heatwave and heavy-precipitation analyses for Guangdong, China in the twenty-first century. Clim. Dyn. 61, 2885–2905. https://doi.org/10.1007/s00382-023-06712-y

Ridder, N.N., Ukkola, A.M., Pitman, A.J., Perkins-Kirkpatrick, S.E., 2022. Increased occurrence of high impact compound events under climate change. npj Clim. Atmos. Sci. 5, 3. https://doi.org/10.1038/s41612-021-00224-4

Salarijazi, M., Ghorbani, K., Mohammadi, M., Ahmadianfar, I., Mohammadrezapour, O., Naser,

M.H., Yaseen, Z.M., 2023. Spatial-temporal estimation of maximum temperature high returns periods for annual time series considering stationary/nonstationary approaches in Iran urban area. Urban Clim. 49, 101504. https://doi.org/10.1016/j.uclim.2023.101504

Samset, B.H., Sand, M., Smith, C.J., Bauer, S.E., Forster, P.M., Fuglestvedt, J.S., Osprey, S., Schleussner, C. -F., 2018. Climate Impacts From a Removal of Anthropogenic Aerosol Emissions. Geophys. Res. Lett. 45, 1020–1029. https://doi.org/10.1002/2017GL076079

Shao, S., Zhang, H., Singh, V.P., Ding, H., Zhang, J., Wu, Y., 2022. Nonstationary analysis of hydrological drought index in a coupled human-water system: Application of the GAMLSS with meteorological and anthropogenic covariates in the Wuding River basin, China. J. Hydrol. 608, 127692. https://doi.org/10.1016/j.jhydrol.2022.127692

Shu, Z., Jin, J., Zhang, J., Wang, G., Lian, Y., Liu, Y., Bao, Z., Guan, T., He, R., Liu, C., Jing, P., 2024. 1.5℃ and 2.0℃ of global warming intensifies the hydrological extremes in China. J. Hydrol. 635, 131229. https://doi.org/10.1016/j.jhydrol.2024.131229

Singh, H., Najafi, M.R., Cannon, A.J., 2021. Characterizing non-stationary compound extreme events in a changing climate based on large-ensemble climate simulations. Clim. Dyn. 56, 1389–1405. https://doi.org/10.1007/s00382-020-05538-2

Sun, F., Roderick, M.L., Farquhar, G.D., 2018. Rainfall statistics, stationarity, and climate change. Proc. Natl. Acad. Sci. U.S.A. 115, 2305–2310. https://doi.org/10.1073/pnas.1705349115

Talbot, C., Bou-Zeid, E., Smith, J., 2012. Nested Mesoscale Large-Eddy Simulations with WRF: Performance in Real Test Cases. J. Hydrometeorol. 13, 1421–1441. https://doi.org/10.1175/JHM-D-11-048.1

Tapiador, F.J., Navarro, A., Moreno, R., Sánchez, J.L., García-Ortega, E., 2020. Regional climate models: 30 years of dynamical downscaling. Atmos. Res. 235, 104785. https://doi.org/10.1016/j.atmosres.2019.104785

Torrez-Rodriguez, L., Goubanova, K., Muñoz, C., Montecinos, A., 2023. Evaluation of temperature and precipitation from CORDEX-CORE South America and Eta-RCM regional climate simulations over the complex terrain of Subtropical Chile. Clim. Dyn. 61, 3195–3221. https://doi.org/10.1007/s00382-023-06730-w

Van Der Wiel, K., Bintanja, R., 2021. Contribution of climatic changes in mean and variability to

monthly temperature and precipitation extremes. Commun. Earth Environ. 2, 1. https://doi.org/10.1038/s43247-020-00077-4

Varga, Á.J., Breuer, H., 2020. Sensitivity of simulated temperature, precipitation, and global radiation to different WRF configurations over the Carpathian Basin for regional climate applications. Clim. Dyn. 55, 2849–2866. https://doi.org/10.1007/s00382-020-05416-x

Wang, S., Chen, X., Yao, H., Ruan, W., Gu, Z., Li, X., Chen, Y., Liu, M., Deng, H., 2024. Separation and spatial variations of typhoon and non-typhoon rainfall at different timescales in typical region of southeast China. Intl. J. Climatol. 44, 4611–4628. https://doi.org/10.1002/joc.8599

Wu, L., Zheng, H., 2023. Regional Climate Effects of Irrigation under Central Asia Warming by 2.0 °C. Remote Sens. 15, 3672. https://doi.org/10.3390/rs15143672

Wu, X., Yang, Y., Jiang, D., 2023. Dramatic increase in the probability of 2006-like compound dry and hot events over Southwest China under future global warming. Weather Clim. Extremes 41, 100592. https://doi.org/10.1016/j.wace.2023.100592

Xie, Y., Sun, W., Ren, M., Chen, S., Huang, Z., Pan, X., 2023. Stacking ensemble learning models for daily runoff prediction using 1D and 2D CNNs. Expert Sys. Appl. 217, 119469. https://doi.org/10.1016/j.eswa.2022.119469

Xu, W., Liu, Z., Gao, L., Lei, X., Zhang, Y., 2025. Changes in Global Marine Heatwaves in a Non-stationary Climate. Geophys. Res. Lett. 52, e2024GL114497. https://doi.org/10.1029/2024GL114497

Xu, Z., Han, Y., Tam, C.-Y., Yang, Z.-L., Fu, C., 2021. Bias-corrected CMIP6 global dataset for dynamical downscaling of the historical and future climate (1979–2100). Sci. Data 8, 293. https://doi.org/10.1038/s41597-021-01079-3

Yang, T., Chen, X., Hamdi, R., Li, Q., Cui, F., Li, L., Liu, Y., De Maeyer, P., Duan, W., 2024. Assessment of snow simulation using Noah-MP land surface model forced by various precipitation sources in the Central Tianshan Mountains, Central Asia. Atmos. Res. 300, 107251. https://doi.org/10.1016/j.atmosres.2024.107251

Yang, X., Yan, Y., Zhou, X., Zhu, L., Ma, M., Zhang, J., Chen, Y., Gao, L., 2025. Risk of Compound Typhoon Disaster Chains: Insights from Southeastern China. Int. J. Disaster Risk Sci. 16, 870–887. https://doi.org/10.1007/s13753-025-00674-x

Yin, C., Ting, M., Kornhuber, K., Horton, R.M., Yang, Y., Jiang, Y., 2025. CETD, a global compound events detection and visualisation toolbox and dataset. Sci. Data 12, 356. https://doi.org/10.1038/s41597-025-04530-x

Yin, H., Zhang, X., Wang, F., Zhang, Y., Xia, R., Jin, J., 2021. Rainfall-runoff modeling using LSTM-based multi-state-vector sequence-to-sequence model. J. Hydrol. 598, 126378. https://doi.org/10.1016/j.jhydrol.2021.126378

Zhang, W., Furtado, K., Wu, P., Zhou, T., Chadwick, R., Marzin, C., Rostron, J., Sexton, D., 2021. Increasing precipitation variability on daily-to-multiyear time scales in a warmer world. Sci. Adv. 7, eabf8021. https://doi.org/10.1126/sciadv.abf8021

Zhang, Y., Deng, C., Xu, W., Zhuang, Y., Jiang, L., Jiang, C., Guan, X., Wei, J., Ma, M., Chen, Y., Peng, J., Gao, L., 2025. Long-term variability of extreme precipitation with WRF model at a complex terrain River Basin. Sci. Rep. 15, 156. https://doi.org/10.1038/s41598-024-84076-x

Zheng, M., Chen, X., Ruan, W., Yao, H., Gu, Z., Geng, K., Li, X., Deng, H., Chen, Y., Liu, M., 2023. Spatiotemporal variation of water cycle components in Minjiang River Basin based on a correction method for evapotranspiration products. J. Hydrol.: Reg. Stud. 50, 101575. https://doi.org/10.1016/j.ejrh.2023.101575

Zhou, P., Tang, J., Ma, M., Ji, D., Shi, J., 2024. High resolution Tibetan Plateau regional reanalysis 1961-present. Sci. Data 11, 444. https://doi.org/10.1038/s41597-024-03282-4

Zscheischler, J., Westra, S., Van Den Hurk, B.J.J.M., Seneviratne, S.I., Ward, P.J., Pitman, A., AghaKouchak, A., Bresch, D.N., Leonard, M., Wahl, T., Zhang, X., 2018. Future climate risk from compound events. Nature Clim. Change 8, 469–477. https://doi.org/10.1038/s41558-018-0156-3